

Gravitational Waves around a Naked Singularity

- *Odd-Parity Perturbation of Lemaître-Tolman-Bondi Space-Time* -

Hideo Iguchi*, Ken-ichi Nakao†, and Tomohiro Harada‡
Department of Physics, Kyoto University, Kyoto 606-8502, Japan

The motion of a spherical dust cloud is described by the Lemaître-Tolman-Bondi solution and is completely specified by initial values of distributions of the rest mass density and specific energy of the dust fluid. From generic initial conditions of this spherically symmetric collapse, there appears a naked singularity at the symmetric center in the course of the gravitational collapse of the dust cloud. So this might be a counter example to the cosmic censorship hypothesis. To investigate the genericity of this example, we examine the stability of the ‘nakedness’ of this singularity against odd-parity modes of non-spherical linear perturbations for the metric, i.e., linear gravitational waves. We find that the perturbations do not diverge but are well-behaved even in the neighborhood of the central naked singularity. This means that the naked singularity formation process is marginally stable against the odd-parity modes of linear gravitational waves.

PACS number(s): 04.20.Dw,04.25.Dm,04.30.Nk

I. INTRODUCTION

The singularity theorems revealed that the occurrence of singularities is a generic property of space-time in general relativity [1–3]. However, those theorems say nothing about the detailed features of the singularities themselves; for example, we do not get information from those theorems about whether the predicted singularity is naked or not. Naked means that the singularity is observable. A singularity is a boundary of space-time. Hence, in order to obtain a solution of hyperbolic field equations for matter, gauge fields and space-time itself in the causal future of a naked singularity, we need to impose a boundary condition on it. However, we do not yet know physically reasonable boundary conditions on singularities and hence to avoid this difficulty, the cosmic censorship hypotheses (CCH) proposed by Penrose [4,5] are often adopted in the analysis of the physical phenomena of the strong gravitational fields.

There are weak and strong versions of the CCH. The weak CCH states that a singularity is covered by an event horizon and never observed by anyone included in the causal past of future null infinity (not globally naked) while the strong CCH says that nobody can observe a singularity (not locally naked). However, the validity of the CCH is one of the most important open questions in classical general relativity. No one has ever proved that these hypotheses hold. On the contrary, some researchers found, analytically or numerically, that there are solutions of the Einstein equations which have naked singularities. If these naked singularities are physically realizable, then we could be in an embarrassing situation because an important assumption in theorems on the nature of a black hole is violated. In the vicinity of a singularity, quantum effects on the space-time will play an important role and therefore if the existence of naked singularities is generic, in order to understand the nature of a black hole, we might need the knowledge of the quantum theory of gravity even if the black hole is a classical entity.

In the last two decades several researchers have shown that the Lemaître-Tolman-Bondi (LTB) space-time [6,7] is one of the candidates for a counter example to both versions of the CCH. This space-time describes the motion of a spherically symmetric inhomogeneous dust cloud and is completely specified by initial values of the rest mass density and specific energy of the dust fluid. Eardley and Smarr showed that the central singularity of the LTB

*e-mail: iguchi@tap.scphys.kyoto-u.ac.jp

†e-mail: nakao@tap.scphys.kyoto-u.ac.jp

‡e-mail: harada@tap.scphys.kyoto-u.ac.jp

space-time can be shell-focusing and naked in the case of marginally bound collapse [8]. Christodoulou showed that the same is true also for the bound case [9]. Newman generalized Christodoulou's analysis to cover a larger class of LTB space-times [10]. Joshi and Dwivedi carried out studies of a much more general class of solutions in which a conical singularity (but not curvature one) was allowed in the initial configuration and showed that the formation of a central naked singularity is a general feature for a very wide range of initial data in the LTB space-time [11]. These results are summarized as follows; in this space-time, a naked singularity appears from generic initial data for *spherically symmetric* configurations of the rest mass density and specific energy of the dust fluid.

In order to recognize this example as a serious counter example to the CCH, we should examine its genericity. That is to say, there is a possibility that the naked singularity is due to physically unrealistic conditions, e.g., assumptions of the spherical symmetry, dust matter and so on. Shapiro and Teukolsky studied evolution of collisionless gas spheroids by fully general relativistic simulations [12]. They found that prolate spheroids with sufficiently elongated initial configurations and even with some angular momentum, may form naked singularities. Ori and Piran numerically examined the structure of self-similar spherical collapse solutions for a perfect fluid with a barotropic equation of state [13]. They showed that there is a globally naked singularity in a significant part of the space of self-similar solutions. Joshi and Dwivedi analytically investigated the self-similar spherically symmetric collapse of a perfect fluid with a similar equation of state [14] and further the naked singularity produced by the gravitational collapse of radiation shells [15] and of more general matter [16].

In this article, we concentrate our attention on the issue whether the spherical symmetry is essential to the occurrence of the shell focusing naked singularity. For this purpose, we consider odd-parity modes of non-spherically symmetric perturbations in the marginally bound LTB space-time and examine the stability of the 'nakedness' of that naked singularity against those linear perturbations. As for the non-spherically symmetric collapse case, Joshi and Krolack revealed that a naked singularity appears also in the Szekeres space-time with an irrotational dust matter [17]. Since the odd-parity perturbations correspond to the rotational motions of the dust fluid and of the space-time itself, our analysis will give a new insight into the formations of naked singularities in non-spherically symmetric space-time.

To decouple physical effects from gauge or coordinate ones, we adopt the gauge-invariant formalism formulated by Gerlach and Sengupta [18] for general spherically symmetric space-times. Here we consider only the metric perturbations, i.e., linear gravitational waves. Using this formalism, we obtain a single decoupled partial differential equation for a gauge-invariant variable corresponding to the odd-parity metric perturbations of the LTB space-time. We analyze this equation numerically by use of single null coordinates, which was adopted by Goldwirth and Piran [19] for the numerical study of spherical collapse of a massless scalar field. Then we shall discuss the stability of the LTB space-time with a central naked singularity from the results of these analyses. A naked singularity is interpreted to be unstable, if perturbations tend to diverge as they approach the naked singularity and the Cauchy horizon associated with it. If such a behavior is found, it means that the perturbations will destroy the Cauchy horizon and change the causal structure of this space-time. Waugh and Lake examined the stability of the central naked singularity of the LTB space-time against perturbations of a massless field by the use of the high-frequency (eikonal) approximation and with the assumption of no back reaction of the massless field to the space-time geometry [20]. Their analysis revealed that the formation of the central naked singularity is stable within the validity of their approximation. In contrast to the analysis by Waugh and Lake, however, the effect of the finite wavelength of the perturbations and the non spherically symmetric dynamics of the space-time itself are taken into account up to the linear order in our present analysis.

This paper is organized as follows. In Section II, we briefly describe the LTB space-time. In Section III, we derive the basic equations for perturbations in the LTB space-time and then give regularity conditions for the perturbations at the symmetric center, which are significant for our stability analysis of the central naked singularity formation. In Section IV, we present the expressions for the perturbations of the Riemann tensor. We show the numerical procedure and results for the marginally bound LTB space-time in Section V. Section VI is devoted to the summary and discussions. We adopt the geometrized units, $c = G = 1$. The signature of the metric tensor and sign convention of the Riemann tensor follow Ref. [21].

II. LEMAÎTRE-TOLMAN-BONDI SPACE-TIME

The inhomogeneous spherically symmetric dust collapse is described by the LTB space-time. Using the synchronous coordinate system, the line element of this space-time is expressed in the form

$$d\bar{s}^2 = \bar{g}_{\mu\nu} dx^\mu dx^\nu \equiv -dt^2 + A^2(t, r) dr^2 + R^2(t, r) (d\theta^2 + \sin^2 \theta d\phi^2). \quad (2.1)$$

The energy-momentum tensor for the dust fluid is

$$\bar{T}^{\mu\nu} = \bar{\rho}(t, r) \bar{u}^\mu \bar{u}^\nu, \quad (2.2)$$

where $\bar{\rho}(t, r)$ is the rest mass density and \bar{u}^μ is the 4-velocity of the dust fluid. In the synchronous coordinate system, the unit normal vector field to the spacelike hypersurfaces is geodesic and there is a freedom of which timelike geodesic field is adopted as the hypersurface unit normal. Using this freedom, we can always set $u^\mu = \delta_0^\mu$ since the 4-velocity of the spherically symmetric dust fluid is tangent to an irrotational timelike geodesic field.

Then the Einstein equations and the equation of motion for the dust fluid reduce to the following simple equations,

$$A = \frac{\partial_r R}{\sqrt{1 + f(r)}}, \quad (2.3)$$

$$\bar{\rho}(t, r) = \frac{1}{8\pi} \frac{1}{R^2} \frac{dF(r)}{\partial_r R \, dr}, \quad (2.4)$$

$$(\partial_t R)^2 - \frac{F(r)}{R} = f(r), \quad (2.5)$$

where $f(r)$ and $F(r)$ are arbitrary functions of the radial coordinate, r . From Eq.(2.4), $F(r)$ is related to the Misner-Sharp mass function [22], $m(r)$, of the dust cloud in the manner

$$m(r) = 4\pi \int_0^{R(t,r)} \bar{\rho}(t, r) R^2 dR = 4\pi \int_0^r \bar{\rho}(t, r) R^2 \partial_r R dr = \frac{F(r)}{2}. \quad (2.6)$$

Hence Eq.(2.5) might be regarded as the energy equation per unit mass. This means that the other arbitrary function, $f(r)$, is recognized as the specific energy of the dust fluid. The motion of the dust cloud is completely specified by the function, $F(r)$, (or equivalently, the initial distribution of the rest mass density, $\bar{\rho}$) and the specific energy, $f(r)$. When we restrict our calculation to the case that the symmetric center, $r = 0$, is initially regular, the central shell focusing singularity is naked if and only if $\partial_r^2 \bar{\rho}|_{r=0} < 0$ is initially satisfied for the marginally bound collapse, $f(r) = 0$ [23,24]. For the collapse that is not marginally bound, there exists a similar condition as an inequality for a value depending on the functional forms of $F(r)$ and $f(r)$ [10,23,24].

III. PERTURBATION METHOD

The perturbation method used in this article is the gauge-invariant one which has been formulated by Gerlach and Sengupta [18] for a general spherically symmetric background space-time. First we briefly review their formalism only for the so-called odd-parity modes. Thereafter we will apply this formalism to the LTB space-time in order to derive the basic equations for our analysis.

The perturbed metric tensor is expressed in the form

$$g_{\mu\nu} = \bar{g}_{\mu\nu} + h_{\mu\nu}, \quad (3.1)$$

where $\bar{g}_{\mu\nu}$ is the metric tensor of the spherically symmetric background space-time and $h_{\mu\nu}$ is a perturbation. The energy-momentum tensor is written in the form

$$T_{\mu\nu} = \bar{T}_{\mu\nu} + \delta T_{\mu\nu}, \quad (3.2)$$

where $\bar{T}_{\mu\nu}$ is a background quantity and $\delta T_{\mu\nu}$ is a perturbation. By virtue of the spherical symmetry of the background space-time, $\bar{T}_{\mu\nu}$ is expressed in the form

$$\bar{T}_{\mu\nu} dx^\mu dx^\nu = \bar{T}_{ab} dx^a dx^b + \frac{1}{2} \bar{T}_B^B R^2(t, r) d\Omega^2, \quad (3.3)$$

where the sub- and superscripts, a, b, \dots represent t and r while A, B, \dots represent θ and ϕ . The odd-parity perturbations of $h_{\mu\nu}$ and $\delta T_{\mu\nu}$ are expressed in the form

$$h_{\mu\nu} = \begin{pmatrix} 0 & 0 & h_0(t, r) \Phi_l^m{}_B \\ & 0 & h_1(t, r) \Phi_l^m{}_B \\ \text{Sym} & & h_2(t, r) \chi_l^m{}_{AB} \end{pmatrix}, \quad (3.4)$$

$$\delta T_{\mu\nu} = \begin{pmatrix} 0 & 0 & t_0(t, r) \Phi_l^m{}_B \\ & 0 & t_1(t, r) \Phi_l^m{}_B \\ \text{Sym} & & t_2(t, r) \chi_l^m{}_{AB} \end{pmatrix}, \quad (3.5)$$

where Φ_{lB}^m and χ_{lAB}^m are odd-parity vector and tensor harmonics associated with the spherical symmetry of the background space-time [25].

We introduce gauge-invariant variables defined by Gerlach and Sengupta. The metric variables are given by

$$k_a = h_a - \frac{1}{2}R^2 \partial_a \left(\frac{h_2}{R^2} \right). \quad (3.6)$$

The matter variables are given by the following combinations,

$$L_a = t_a - \frac{1}{2}T_B^B h_a, \quad (3.7)$$

$$L = t_2 - \frac{1}{2}T_B^B h_2. \quad (3.8)$$

Then the Einstein equations lead to the equations for the metric variables as

$$k^a{}_{|a} = 16\pi L \quad (l \geq 2), \quad (3.9)$$

$$(R^4 W^{ab})_{|b} + (l-1)(l+2)k^a = 16\pi R^2 L^a \quad (l \geq 1), \quad (3.10)$$

where W_{ab} is defined as

$$W_{ab} \equiv \left(\frac{h_b}{R^2} \right)_{|a} - \left(\frac{h_a}{R^2} \right)_{|b} = \left(\frac{k_b}{R^2} \right)_{|a} - \left(\frac{k_a}{R^2} \right)_{|b}, \quad (3.11)$$

and the vertical bar refers to the covariant derivative within the 2-dimensional sub-space-time (t, r) . From the equation of motion for the matter, we get

$$(R^2 L^a)_{|a} = (l-1)(l+2)L \quad (l \geq 1). \quad (3.12)$$

Now we apply the above formalism to the case of the background LTB space-time. From Eqs.(2.2) and (3.5), we find that there is no density perturbation and that only the perturbation of 4-velocity, δu_μ , exists;

$$\delta u_\mu = (0, 0, U(t, r)\Phi_{lB}^m). \quad (3.13)$$

Therefore the odd-parity gauge-invariant matter variables become

$$L_0 = \bar{\rho}U \quad \text{and} \quad L_1 = L = 0. \quad (3.14)$$

From Eqs.(3.9) and (3.10), we obtain the equations of motion for the metric variables,

$$\partial_t (Ak_0) - \partial_r \left(\frac{k_1}{A} \right) = 0, \quad (3.15)$$

$$\partial_r (R^4 \psi_s) + A(l-1)(l+2)k_0 = 16\pi AR^2 L_0, \quad (3.16)$$

$$\partial_t (R^4 \psi_s) + \frac{1}{A}(l-1)(l+2)k_1 = 0, \quad (3.17)$$

where we have introduced another gauge-invariant variable, ψ_s , defined as

$$\psi_s \equiv \frac{1}{A} \left[\partial_t \left(\frac{k_1}{R^2} \right) - \partial_r \left(\frac{k_0}{R^2} \right) \right]. \quad (3.18)$$

Eq.(3.12) becomes

$$\partial_t (AR^2 L_0) = 0. \quad (3.19)$$

This equation is easily integrated and we obtain

$$AR^2 L_0 = \frac{dJ(r)}{dr}, \quad (3.20)$$

where $J(r)$ is an arbitrary function depending only on r . From Eqs.(3.16), (3.17), and (3.20), we obtain a single decoupled wave equation in the form

$$\partial_t \left(\frac{A}{R^2} \partial_t (R^4 \psi_s) \right) - \partial_r \left(\frac{1}{AR^2} \partial_r (R^4 \psi_s) \right) + (l-1)(l+2) A \psi_s = -16\pi \partial_r \left(\frac{1}{AR^2} \frac{dJ}{dr} \right). \quad (3.21)$$

The variable, ψ_s , differs from the gauge-invariant variable used in Ref. [26] by a factor of $1/R^2$. The reason why we adopt ψ_s as a gauge-invariant variable instead is due to regularity conditions at $r = 0$. Further, as will be shown later, ψ_s is closely connected with the curvature tensor near the center.

Let us consider the regularity conditions for the background metric functions and gauge-invariant perturbations at $r = 0$. Hereafter we restrict ourselves to the axisymmetric case, i.e., $m = 0$. Note that this restriction does not lose generality of our analysis. Further we consider only the case in which the space-time is regular before the occurrence of the singularity. This means that, before the naked singularity formation, the metric functions, $R(t, r)$ and $A(t, r)$, behave near the center in the manner

$$R \longrightarrow R_c(t)r + O(r^3), \quad (3.22)$$

$$A \longrightarrow R_c(t) + O(r^2). \quad (3.23)$$

To investigate the regularity conditions of the gauge-invariant variables, k_a and L_0 , we follow Bardeen and Piran [27]. The results are given by

$$L_0 \longrightarrow L_c(t)r^{l+1} + O(r^{l+3}), \quad (3.24)$$

$$k_0 \longrightarrow k_{0c}(t)r^{l+1} + O(r^{l+3}), \quad (3.25)$$

$$k_1 \longrightarrow k_{1c}(t)r^{l+2} + O(r^{l+4}). \quad (3.26)$$

From Eqs.(3.18), (3.22), (3.23),(3.25) and (3.26), we find that ψ_s behaves near the center as

$$\psi_s \longrightarrow \psi_{sc}(t)r^{l-2} + O(r^l) \quad \text{for } l \geq 2, \quad (3.27)$$

$$\psi_s \longrightarrow \psi_{sc(t)}r + O(r^3) \quad \text{for } l = 1. \quad (3.28)$$

In the case of $l \geq 2$, the coefficient, $\psi_{sc}(t)$, is related to $R_c(t)$ and $k_{0c}(t)$ in the manner

$$\psi_{sc}(t) = -(l-1) \frac{k_{0c}(t)}{R_c^3(t)}. \quad (3.29)$$

From the above equations, we note that only the quadrupole mode, $l = 2$, of ψ_s does not vanish at the center.

IV. PERTURBATION OF RIEMANN TENSOR

In this section, we consider the perturbation of the Riemann tensor, $R_{\mu\nu\sigma}{}^\lambda$, of the LTB space-time to investigate the relation between the singularity formation and the perturbations. The Riemann tensor is decomposed into the Ricci tensor, $R_{\mu\nu}$, and the Weyl tensor,

$$C_{\mu\nu\sigma\lambda} = R_{\mu\nu\sigma\lambda} + \{g_{\mu[\lambda}R_{\sigma]\nu} + g_{\nu[\sigma}R_{\lambda]\mu}\} + \frac{1}{3}Rg_{\mu[\sigma}g_{\lambda]\nu}. \quad (4.1)$$

We shall give them in the form of the components of the following tetrad basis,

$$e_{(t)}^\mu = \left(1, 0, 0, -\frac{h_0 P_{l,\theta}}{R^2 \sin \theta} \right), \quad (4.2)$$

$$e_{(r)}^\mu = \left(0, \frac{1}{A}, 0, -\frac{h_1 P_{l,\theta}}{AR^2 \sin \theta} \right), \quad (4.3)$$

$$e_{(\theta)}^\mu = \left(0, 0, \frac{1}{R}, -\frac{h_2}{2R^3 \sin^2 \theta} (\sin \theta P_{l,\theta,\theta} - \cos \theta P_{l,\theta}) \right), \quad (4.4)$$

$$e_{(\phi)}^\mu = \left(0, 0, 0, \frac{1}{R \sin \theta} \right), \quad (4.5)$$

where $P_l(\cos\theta)$ is the Legendre polynomial and the comma followed by θ denotes a derivative with respect to θ . The Weyl tensor is then decomposed into the so-called electric part, $E_{\alpha\beta}$, and magnetic part, $B_{\alpha\beta}$, which are defined as

$$E_{\alpha\beta} \equiv C_{\alpha\mu\beta\nu} e_{(t)}^\mu e_{(t)}^\nu, \quad (4.6)$$

$$B_{\alpha\beta} \equiv \frac{1}{2} \epsilon_{\alpha\sigma}{}^{\mu\nu} C_{\mu\nu\beta\lambda} e_{(t)}^\sigma e_{(t)}^\lambda, \quad (4.7)$$

where $\epsilon_{\mu\nu\alpha\beta}$ is the 4-dimensional skew tensor. In the background LTB space-time, the Ricci tensor has a non-zero value in the region of non-vanishing rest mass density, $\bar{\rho} \neq 0$, through the Einstein equations and also the electric part has a non-zero value. On the other hand, the magnetic part is identically equal to zero in the background LTB space-time. However, when axisymmetric odd-parity metric perturbations exist, the Riemann tensor is perturbed and the magnetic part may also have a non-vanishing value.

The perturbation of the Ricci tensor is expressed by the matter perturbation through the Einstein equations as

$$\delta(R_{(t)(\phi)}) = \frac{8\pi}{R} L_0 P_{l,\theta} = \frac{8\pi}{AR^3} \frac{dJ}{dr} P_{l,\theta}, \quad (4.8)$$

and the other components vanish, where we have used Eq.(3.20) in the last equality. The perturbations of the tetrad components of the electric part are given in the form

$$\delta(E_{(r)(\phi)}) = \frac{1}{2} \left[\frac{1}{AR^3} (l-1)(l+2)k_1 + R(\partial_t R)\psi_s \right] \sin\theta P_{l,\theta}, \quad (4.9)$$

$$\delta(E_{(\theta)(\phi)}) = \frac{1}{2AR^2} \left[\partial_t \left(\frac{k_1}{A} \right) - (\partial_t A)k_0 \right] (\sin\theta P_{l,\theta,\theta} - \cos\theta P_{l,\theta}), \quad (4.10)$$

and the other components vanish. The perturbations of the tetrad components of the magnetic part are obtained in the form

$$\delta(B_{(r)(r)}) = \frac{1}{2} l(l+1) \psi_s P_l, \quad (4.11)$$

$$\delta(B_{(r)(\theta)}) = \frac{1}{4AR^3} [R^2 \partial_r (R^2 \psi_s) - A(l-1)(l+2)k_0] P_{l,\theta}, \quad (4.12)$$

$$\begin{aligned} \delta(B_{(\theta)(\theta)}) &= -\frac{1}{AR^2} \left[R \partial_r \left(\frac{k_0}{R} \right) + \left(\frac{\partial_t R}{R} - \frac{\partial_t A}{A} \right) k_1 + \frac{1}{2} AR^2 \psi_s \right] P_{l,\theta,\theta} \\ &\quad - \frac{1}{2AR^2} \left[R \partial_r \left(\frac{k_0}{R} \right) + \left(\frac{\partial_t R}{R} - \frac{\partial_t A}{A} \right) k_1 + AR^2 \psi_s \right] l(l+1) P_l, \end{aligned} \quad (4.13)$$

$$\begin{aligned} \delta(B_{(\phi)(\phi)}) &= -\frac{1}{AR^2} \left[R \partial_r \left(\frac{k_0}{R} \right) + \left(\frac{\partial_t R}{R} - \frac{\partial_t A}{A} \right) k_1 + \frac{1}{2} AR^2 \psi_s \right] \cot\theta P_{l,\theta} \\ &\quad - \frac{1}{2AR^2} \left[R \partial_r \left(\frac{k_0}{R} \right) + \left(\frac{\partial_t R}{R} - \frac{\partial_t A}{A} \right) k_1 + AR^2 \psi_s \right] l(l+1) P_l, \end{aligned} \quad (4.14)$$

and the other components vanish.

Now we will investigate the behavior of the Ricci and Weyl tensors near the center where the naked singularity appears. From the regularity conditions (3.22)-(3.29), we can see that the perturbations of the Ricci and Weyl tensors obtained in the above behave near the center in the manner

$$\delta(R_{(t)(\phi)}) \longrightarrow \frac{8\pi}{R_c} L_c P_{l,\theta} r^l, \quad (4.15)$$

for the Ricci tensor, and

$$\delta(E_{(r)(\phi)}) \longrightarrow \frac{1}{2R_c^4} (l-1) \left[(l+2)k_{1c} - R_c \frac{dR_c}{dt} k_{0c} \right] P_{l,\theta} r^{l-1}, \quad (4.16)$$

$$\delta(E_{(\theta)(\phi)}) \longrightarrow \frac{1}{2R_c^4} \left[(l+2)k_{1c} - R_c \frac{dR_c}{dt} k_{0c} \right] (P_{l,\theta,\theta} - \cot\theta P_{l,\theta}) r^{l-1}, \quad (4.17)$$

$$\delta(B_{(r)(r)}) \longrightarrow -\frac{1}{2R_c^3} (l-1)l(l+1)k_{0c} P_l r^{l-2}, \quad (4.18)$$

$$\delta(B_{(r)(\theta)}) \longrightarrow -\frac{1}{2R_c^3}(l-1)(l+1)k_{0c}P_{l,\theta}r^{l-2}, \quad (4.19)$$

$$\delta(B_{(\theta)(\theta)}) \longrightarrow -\frac{1}{2R_c^3}(l+1)k_{0c}(P_{l,\theta,\theta} + lP_l)r^{l-2}, \quad (4.20)$$

$$\delta(B_{(\phi)(\phi)}) \longrightarrow -\frac{1}{2R_c^3}(l+1)k_{0c}(\cot\theta P_{l,\theta} + lP_l)r^{l-2}, \quad (4.21)$$

for the Weyl tensor of $l \geq 2$. For the $l = 1$ mode, we find

$$\delta(E_{(r)(\phi)}) \longrightarrow \frac{1}{2} \frac{dR_c}{dt} \psi_{sc} r^2 \sin\theta, \quad (4.22)$$

$$\delta(B_{(r)(r)}) \longrightarrow -\psi_{sc} r \cos\theta, \quad (4.23)$$

$$\delta(B_{(r)(\theta)}) \longrightarrow \frac{1}{4} \psi_{sc} r \sin\theta, \quad (4.24)$$

$$\delta(B_{(\theta)(\theta)}) \longrightarrow \frac{1}{2} \psi_{sc} r \cos\theta, \quad (4.25)$$

$$\delta(B_{(\phi)(\phi)}) = \delta(B_{(\theta)(\theta)}). \quad (4.26)$$

From the above equations, we see that the perturbations of the tetrad components of the Ricci and Weyl tensors, except for the quadrupole mode, $l = 2$, of the magnetic part, $B_{\alpha\beta}$, identically vanish at the center. This means that the central naked singularity formation is affected only by the quadrupole mode up to linear order. Therefore, hereafter we shall consider the quadrupole mode only. On the other hand, since the solution for the dipole mode, $l = 1$, is obtained analytically, we present it in Appendix A, although the dipole mode vanishes at the center from the regularity condition and does not influence the formation of the central naked singularity up to linear order.

V. NUMERICAL RESULTS AND DISCUSSIONS

Here we will perform numerical integration of Eq.(3.21) for the quadrupole mode, $l = 2$. As mentioned above, the gauge-invariant matter perturbation variable, L_0 , and the perturbation of the Ricci tensor vanish at the regular center. Here we restrict our investigation to the case of no matter perturbations, namely the right hand side of Eq.(3.21) vanishes. The non-vanishing matter perturbation case should be investigated in future. Further, for the simplicity of calculations, we consider only the marginally bound case, $f(r) = 0$, as background space-time.

By virtue of $f(r) = 0$, we can easily integrate Eq.(2.5) and obtain

$$R(t, r) = \left(\frac{9F}{4}\right)^{1/3} [t_0(r) - t]^{2/3}, \quad (5.1)$$

where $t_0(r)$ is an arbitrary function of r . Using the freedom for the scaling of r , we choose $R(0, r) = r$. This scaling of r corresponds to the following choice of $t_0(r)$,

$$t_0(r) = \frac{2}{3\sqrt{F}} r^{3/2}. \quad (5.2)$$

Here note that, from Eq.(2.3), the background metric variable, A , is equal to $\partial_r R$.

Then, the wave equation (3.21) becomes as follows,

$$\begin{aligned} \frac{\partial^2 \psi_s}{\partial t^2} - \frac{1}{(\partial_r R)^2} \frac{\partial^2 \psi_s}{\partial r^2} &= \frac{1}{(\partial_r R)^2} \left(6 \frac{\partial_r R}{R} - \frac{\partial_r^2 R}{\partial_r R} \right) \frac{\partial \psi_s}{\partial r} - \left(6 \frac{\partial_t R}{R} + \frac{\partial_t \partial_r R}{\partial_r R} \right) \frac{\partial \psi_s}{\partial t} \\ &\quad - 4 \left[\left(\frac{\partial_t \partial_r R}{\partial_r R} \right) \frac{\partial_t R}{R} + \left(\frac{\partial_t R}{R} \right)^2 + \frac{\partial_t^2 R}{R} \right] \psi_s. \end{aligned} \quad (5.3)$$

We solve this partially differential equation numerically. In the rest of this section, we explain the details of the background space-time considered here, numerical methods and boundary conditions. Further we show the numerical results.

A. Background Density Profile

The background space-time and the motion of the marginally bound dust cloud are completely determined by the initial rest mass density profile, $\bar{\rho}(0, r)$. Further as already mentioned, it should satisfy the condition $\partial_r^2 \bar{\rho}|_{r=0} < 0$ in order that the central naked singularity is formed. We, therefore, adopt the following initial rest mass density profile so that the central naked singularity appears;

$$\bar{\rho}(0, r) = \begin{cases} \rho_0[1 - 2(r/r_b)^2 + (r/r_b)^4] & \text{for } 0 \leq r \leq r_b \\ 0 & \text{for } r > r_b, \end{cases} \quad (5.4)$$

where ρ_0 is a positive constant and r_b denotes the radial coordinate at the surface of the dust cloud. The total (gravitational) mass of the dust cloud is

$$M = m(r_b) = \frac{32\pi}{105} \rho_0 r_b^3. \quad (5.5)$$

The time of the central naked singularity formation is

$$t = t_0(0) = \frac{1}{\sqrt{6\pi\rho_0}}. \quad (5.6)$$

Whether the naked singularity is global or local is determined by a non-dimensional constant $\rho_0 r_b^2$. It is known that the singularity is globally naked for sufficiently small $\rho_0 r_b^2$ [9,23]. However, the critical value of $\rho_0 r_b^2$ can not be obtained explicitly. Hence, after $\rho_0 r_b^2$ is given, we have to investigate whether the central naked singularity is global or local, by numerically solving the future directed null ray from the central naked singularity. Here we consider two cases. One is that of $\rho_0 r_b^2 = 3 \times 10^{-2}$, which corresponds to a globally naked singularity, and the other is that of $\rho_0 r_b^2 = 3 \times 10^{-1}$, which corresponds to a locally naked one.

In the globally naked case, the initial radius of the dust cloud and the time of the central naked singularity formation are given by

$$\frac{R(0, r_b)}{M} = \frac{r_b}{M} = \frac{105}{32\pi\rho_0 r_b^2} \cong 34.8, \quad (5.7)$$

$$\frac{t_0(0)}{M} = \frac{105}{32\sqrt{6}\pi^{3/2}(\rho_0 r_b^2)^{3/2}} \cong 46.3. \quad (5.8)$$

On the other hand, in the locally naked case, they are given by

$$\frac{R(0, r_b)}{M} = \frac{r_b}{M} \cong 3.48, \quad (5.9)$$

$$\frac{t_0(0)}{M} \cong 1.46. \quad (5.10)$$

B. Numerical Procedure

Next, we describe the procedure of our numerical calculation. We have a disadvantage when we use the (t, r) coordinate system, because of the restriction on the region in which we can numerically construct the solution of the wave equation, (3.21). Therefore, instead of the (t, r) coordinate system, we introduce a single-null coordinate system, (u, r') , where u is an out-going null coordinate and chosen so that it agrees with t at the symmetric center and we choose $r' = r$. We perform the numerical integration along two characteristic directions. The transformation matrix is formally expressed in the form

$$dr' = dr, \quad (5.11)$$

$$du = (\partial_t u)_r dt + (\partial_r u)_t dr. \quad (5.12)$$

Because u is the out-going null coordinate, the following relation holds,

$$\frac{(\partial_t u)_r}{(\partial_r u)_t} = -\frac{1}{\partial_r R}. \quad (5.13)$$

Using these relations, we obtain the line element of the 2-dimensional sub-space-time, (t, r) , in the following new form

$$ds_{(2)}^2 = -\alpha^2 du^2 - 2\alpha(\partial_r R) du dr', \quad (5.14)$$

where we have introduced

$$\alpha \equiv \frac{1}{(\partial_t u)_r}. \quad (5.15)$$

Furthermore, from Eqs.(5.11) and (5.12), we obtain

$$\partial_{r'} = -\frac{(\partial_r u)_t}{(\partial_t u)_r} \partial_t + \partial_r = (\partial_r R) \partial_t + \partial_r, \quad (5.16)$$

where we have used Eq.(5.13) in the last equality. The above equation describes that $\partial_{r'}$ is parallel to the future directed out-going null direction.

By using this new coordinate system, (u, r') , Eq.(5.3) is expressed in the form

$$\begin{aligned} \frac{d\phi_s}{du} &= -\frac{\alpha}{R} \left[3\partial_r R + \frac{1}{2}R(\partial_t R)\partial_t \partial_r R - (\partial_t R)^2 \partial_r R + \frac{1}{2}R(\partial_r R)\partial_t^2 R \right] \psi_s \\ &\quad - \frac{\alpha}{2} \left[\frac{\partial_r^2 R}{(\partial_r R)^2} - \frac{2}{R}(1 - \partial_t R) \right] \phi_s, \end{aligned} \quad (5.17)$$

$$\partial_{r'} \psi_s = \frac{1}{R} \phi_s - 3 \frac{\partial_r R}{R} (1 + \partial_t R) \psi_s, \quad (5.18)$$

where the ordinary derivative in the left hand side of Eq.(5.17) is given by

$$\frac{d}{du} = \partial_u + \frac{dr'}{du} \partial_{r'} = \partial_u - \frac{\alpha}{2\partial_r R} \partial_{r'}, \quad (5.19)$$

and we have introduced a new variable, ϕ_s , given by Eq.(5.18).

The procedure of the numerical integration is as follows. At the first step, we prepare initial data corresponding to imploding waves for ϕ_s at each grid point on the initial null hypersurface labeled by $u = u_0 = \text{constant}$. Then, using this ϕ_s , ψ_s is obtained at each grid point on $u = u_0$ by the integration of Eq.(5.18). At the next step, in order to obtain ϕ_s at each grid point on $u = u_0 + \Delta u$, we integrate Eq.(5.17) by using values of ϕ_s and ψ_s on $u = u_0$. Then, ψ_s on $u = u_0 + \Delta u$ is obtained from Eq.(5.18) by using ϕ_s on $u = u_0 + \Delta u$. We repeat this procedure and obtain a solution outside the Cauchy horizon associated with the central naked singularity.

In the above procedure, we should impose a boundary condition on ψ_s at the center to perform the numerical integration of Eq.(5.18). From Eqs.(3.27) and (3.29), in the case of $l = 2$ mode, ψ_s behaves in the manner

$$\psi_s \longrightarrow -\frac{k_{0c}(t)}{R_c^3(t)} + O(r^2) \quad \text{for } r \longrightarrow 0. \quad (5.20)$$

Hence, we have to numerically make ψ_s near the center so that Eq.(5.20) is guaranteed on a surface of $t = \text{constant}$, and this leads to the boundary condition for ψ_s at the center.

Here we comment on our numerical code. We compared the numerical results for the Minkowski space-time with the analytical solutions which will be described in the next subsection. In this case, the result produced by our code agreed with the analytical solution very closely. Another check we performed was to compare the numerical results for several mesh sizes with each other. This test confirmed that our numerical results were almost independent of the mesh size.

C. Initial Conditions and Numerical Results

The initial conditions which we consider are a Gaussian-shaped wave packet with respect to the coordinate, r' ,

$$\psi_s|_{u=u_0} = \psi_s^i \exp \left[-\frac{(r' - r'_c)^2}{2\sigma^2} \right], \quad (5.21)$$

where ψ_s^i , σ , and r'_c are constants and characterize the amplitude, width and initial position of the initial wave packet, respectively. The initial null hypersurface, $u = u_0$, is chosen so that it includes a world point $(t, r) = (0, 0)$, except for the analysis of the scattered waves which will be discussed in this section.

We investigate models with three different initial positions of the wave packet, i.e., r'_c in Eq.(5.21), on the initial null hypersurface. In Case 1, the wave packet reaches the center of the dust cloud before the formation of the central naked singularity. In Case 2, a significant portion of the wave packet hits the central naked singularity. In Case 3, the packet does not hit the central naked singularity but reaches the Cauchy horizon associated with it. Fig.1 shows these situations schematically. In each case, the value of ψ_s at the center is plotted as a function of the coordinate time, t , in Fig.2 for the globally naked case and in Fig.3 for the locally naked case. Note that it is impossible to perform the numerical calculation in the causal future of the central naked singularity. Therefore we plot ψ_s at the center only before the occurrence of the central naked singularity. Although such a difficulty exists, we find that violent growth of the amplitude of ψ_s is not observed near the central naked singularity and Cauchy horizon associated with it.

Next we show the dependence of ψ_s at the center on the width of the initial wave packet. Fig.4 depicts ψ_s at the center for various widths of packets in Case 2. It is found that the amplitude of ψ_s with smaller initial width becomes larger at the center. The relation between the width, σ , and the maximal value of $|\psi_s|$ at the center is shown in Fig.5. We find that there is the following power-law relation

$$|\psi_s|_{r=0} \propto \sigma^{-3}. \quad (5.22)$$

We also observe the time dependence of ψ_s along the line of a constant circumferential radius outside the dust cloud. Since we would like to see the effect of the central naked singularity on ψ_s , we consider the globally naked case only. We set up an initial wave packet of $\sigma = 0.05r_b$ at $R = 100M$ on the initial null hypersurface which does not include the space-time point $(t, r) = (0, 0)$ but is chosen so that the wave packet will reach the neighborhood of the central naked singularity.

The results are shown in Fig.6 in which ψ_s at $R = 100M$ is plotted as a function of t . Note that the point, $R = 100M$, is located in the vacuum region which is the Schwarzschild space-time by Birkhoff's theorem. Hence the value of t along the curve of $R = 100M$ agrees with that of the usual static time coordinate of the Schwarzschild space-time.

In Fig.6(a), the solid line corresponds to Case 1 while the broken line is for Case 2. The dotted line denotes the result for Case 3. The left-hand peaks in Fig.6(a) correspond to the initial incident waves. On the other hand, the right-hand peaks of Cases 1 and 2 in this figure correspond to the scattered outgoing waves. In Case 3, the right-hand peak does not exist and this is because, in this case, almost all portions of the incident waves enter into the Cauchy horizon associated with the central naked singularity and hence it is impossible to follow numerically the scattered waves in the causal future of the central naked singularity. Fig.6(b) shows detailed behavior of the scattered ψ_s for Case 2. It is a most important fact seen in these figures that the amplitude of the scattered waves is almost the same as that of the initial incident waves in Cases 1 and 2.

In order to investigate the effect of the wavelength of ψ_s , we perform the numerical integration for Case 2 but with different initial widths of wave packets. The results of narrower ($\sigma = 0.02r_b$) and broader ($\sigma = 0.25r_b$ and $0.5r_b$) widths than the case plotted in Fig.6(a) and (b) are shown in Fig.6(c). The narrower wave is similar to $\sigma = 0.05r_b$ while the broader packets have different forms of scattered waves from the narrower one. However, in both cases, the amplitude of the scattered wave is not so different from the incident one.

D. Minkowski Case

Here we investigate the behavior of ψ_s in the Minkowski space-time and compare it with the results of the LTB space-time obtained in the above in order to reveal the effects of the existence of the dust cloud and the central naked singularity on the dynamics of ψ_s . In the Minkowski case, since $R(t, r) = r$, Eq.(5.3) becomes

$$\partial_t^2 \psi_s - \partial_r^2 \psi_s = \frac{6}{r} \partial_r \psi_s. \quad (5.23)$$

The solution of this equation which is regular at $r = 0$ is obtained in the form

$$\psi_s = 3 \frac{f(t-r) - f(t+r)}{r^5} + 3 \frac{f^{(1)}(t-r) + f^{(1)}(t+r)}{r^4} + \frac{f^{(2)}(t-r) - f^{(2)}(t+r)}{r^3}, \quad (5.24)$$

where $f(x)$ is an arbitrary function and $f^{(n)}(x)$ denotes the n -th order derivative of $f(x)$ with respect to x . We set the following initial wave packet on the null hypersurface, $t = r$,

$$\psi_s = \exp \left[-\frac{(r - r_c)^2}{2\sigma^2} \right]. \quad (5.25)$$

Using the above solution, we compare the evolution of wave forms in the Minkowski space-time with that in the LTB space-time. The initial wave packet in the LTB space-time has been given by Eq.(5.21) as a function of the coordinate radius, r' . However, note that r' does not agree with the circumferential radius, R , in this case but in the Minkowski case, the coordinate radius, r , agrees with the circumferential radius, R . Since the circumferential radius, R , is tightly connected with the behavior of the amplitude of the wave, we should set the same initial data with respect to R both for the LTB and Minkowski cases. Hence first we plot the initial wave packet (5.21) as a function of R/M on the initial null hypersurface and then the values of σ and r_c in Eq.(5.25) are adjusted so that the initial wave form fits well with that of the LTB case.

First we consider the evolution of ψ_s at the center. Using Eqs.(5.24) and (5.25), we obtain ψ_s at the center in the form

$$\begin{aligned} \psi_s(t, 0) = & \left[1 - \frac{1}{\sigma^2} \left(\frac{t}{2} - r_c \right) \frac{t}{2} - \frac{1}{4\sigma^2} \left(\frac{t}{2} \right)^2 + \frac{1}{4\sigma^4} \left(\frac{t}{2} - r_c \right)^2 \left(\frac{t}{2} \right)^2 \right. \\ & \left. + \frac{1}{20\sigma^4} \left(\frac{t}{2} - r_c \right) \left(\frac{t}{2} \right)^3 - \frac{1}{60\sigma^6} \left(\frac{t}{2} - r_c \right)^3 \left(\frac{t}{2} \right)^3 \right] \exp \left[-\frac{1}{2\sigma^2} \left(\frac{t}{2} - r_c \right)^2 \right]. \end{aligned} \quad (5.26)$$

The parameters, σ and r_c , in Eq.(5.25) are chosen so that the initial wave packets fit well with those of the Cases 1 and 2 of Fig2. The results are given in Fig.7(a) and (b), respectively, and in this figure, we also plot the results for the corresponding cases of the LTB space-time. It should be noted that there is scarcely any difference between the wave forms of the Minkowski and LTB cases.

Next we consider the behavior of ψ_s at a finite circumferential radius which agrees with the numerical value of $R = 100M$ in the LTB case. Here the wave form is obtained numerically by the same procedure as in the LTB case. The result is shown in Fig.8. We also plot the corresponding case of the LTB space-time in the same figure. We find that there is a little difference of the phase between the Minkowski and LTB cases. However, the behavior of ψ_s in the Minkowski case is basically the same as that in the LTB case. The effect due to the dust cloud and the existence of the central naked singularity on the propagation of ψ_s is rather small.

We consider the relation between the maximum value of $|\psi_s|$ observed at the center and the width, σ , of an initial wave packet in the Minkowski space-time. This relation is obtained from Eq.(5.26). The results are also shown in Fig.5. The power-law relation Eq.(5.22) is also valid in the Minkowski case. From Eq.(5.24), ψ_s is approximately proportion to $1/r^3$ except for the region of $r \lesssim \sigma$ around the center. If the initial amplitude of the wave packet has a value ψ_i at $r = r_c$, then the value of ψ_s at $r = \sigma$ is roughly estimated as $\psi_i \times (\sigma/r_c)^{-3}$. This will be the reason why the relation (5.22) holds in the Minkowski space-time. As we have discussed above, ψ_s behaves outside the Cauchy horizon of the LTB space-time in approximately the same manner as in the Minkowski space-time. Therefore it would be also the reason why the relation (5.22) holds in the LTB space-time.

As a result, we conclude that even in the neighborhood of the central naked singularity and of the Cauchy horizon associated with it, the metric perturbation, ψ_s , does not show any peculiar behavior. However, we should note that ψ_s does not vanish in the neighborhood of the central naked singularity although it is well-behaved. Therefore, the formation process of the central naked singularity is *marginally stable* against the odd-parity metric perturbations.

VI. CONCLUSIONS

We have investigated the behavior of the odd-parity linear perturbations in the LTB space-time. We have derived the wave equation for the gauge-invariant variable, ψ_s . From the analysis of the regularity for ψ_s and the perturbations of the Riemann tensor, only the quadrupole mode, $l = 2$, of ψ_s and of the magnetic part of the Weyl tensor does not vanish at the symmetric center of the background LTB space-time, where a naked singularity appears in the course of the gravitational collapse of the dust cloud. Therefore this quadrupole mode is the most important for the stability analysis of naked singularity formation in the LTB space-time. Then we have performed numerical experiments on how a Gaussian-shaped incident wave packet behaves under this wave equation for the $l = 2$ mode without matter perturbations. From those numerical experiments, we have obtained the following results. When this wave packet approaches the center, its amplitude becomes larger but finite. The amplitude at the center depends on the width of the initial wave packet according to a power law. On the other hand, when the incident wave packet initially located outside the dust cloud returns back to the same circumferential radius as the initial one, the amplitude of the returned wave is almost equal to that of the incident one.

In order to reveal the characteristic effects of the LTB space-time on the behavior of ψ_s , we have also investigated ψ_s in the Minkowski space-time. Then we have found that in the outside of the Cauchy horizon associated with the central naked singularity, the behavior of ψ_s in the LTB space-time seems to be not so different from that in the Minkowski space-time at least except for the extreme neighborhood of the naked singularity. Therefore the power-law dependence in the LTB space-time described above is basically realized by the analytical discussion about the case of the Minkowski space-time. Further the propagation effect due to the existence of the dust cloud and the occurrence of the central naked singularity is rather small. In other words, there is no peculiar behavior of ψ_s even in the neighborhood of the central naked singularity. However, it should be noted that the odd-parity metric perturbation does not vanish in the neighborhood of the central naked singularity and Cauchy horizon associated with it. As a result, we conclude that the central naked singularity formation in the LTB space-time is ‘marginally’ stable against the odd-parity metric perturbations.

We note that our analyses are not sufficient to determine the stability of the naked singularity formation in the LTB space-time. There remain some problems to complete the analysis. The first problem is to take account of odd-parity matter perturbations. We are now investigating this problem. The second is to consider the even-parity mode in which the metric and matter perturbations are essentially coupled with each other. This problem will be analyzed in future. In this paper, we have dealt with the marginally bound case. For the case that is not marginally bound collapse, the condition of the appearance of the central naked singularity is slightly different from the above case [23,24] and hence there is a possibility that the behavior of ψ_s in this case is different from the marginally bound one. This case is now under investigation.

ACKNOWLEDGMENTS

We would like to thank T. Nakamura, M. Sasaki, M. Shibata, T. Tanaka, M. Siino and T. Chiba for helpful and useful discussions, and N. Sugiyama and S. A. Hayward for a careful reading of the manuscript. We are also grateful to H. Sato and colleagues in the theoretical astrophysics group in Kyoto University for useful comments and encouragement.

APPENDIX A: ANALYTIC SOLUTION OF THE DIPOLE MODE

We present an analytic solution of the wave equations for the $l = 1$ mode. Substituting $l = 1$ into Eqs.(3.16) and (3.17), we get

$$\partial_t (R^4 \psi_s) = 0, \tag{A1}$$

$$\partial_r [R^4 \psi_s - 16\pi J(r)] = 0. \tag{A2}$$

Eq.(A2) is easily integrated and we obtain

$$R^4 \psi_s - 16\pi J(r) = c(t), \tag{A3}$$

where $c(t)$ is an arbitrary function of t . Substituting this equation into (A1), we obtain

$$\partial_t c(t) = 0. \tag{A4}$$

Hence the function, $c(t)$, is temporally constant. From Eq.(3.20) and the regularity conditions for R , L_0 and ψ_s , the left hand side of Eq.(A3) vanishes at the center. Therefore the function, $c(t)$, should vanish identically and the solution for the dipole mode is obtained in the form

$$\psi_s = \frac{16\pi}{R^4} J(r). \tag{A5}$$

From the regularity condition, (3.28), $J(r)/R^4$, is identically zero at the regular center and hence this mode does not affect the formation of the central naked singularity.

- [1] R. Penrose, Phys. Rev. Lett. **14**, 57 (1965).
- [2] S.W. Hawking, Proc. R. Soc. London, Ser. **A300**, 187 (1967).
- [3] S.W. Hawking and R. Penrose, Proc. R. Soc. London, Ser. **A314**, 529 (1970).
- [4] R. Penrose, Riv. Nuovo Cimento **1**, 252 (1969).
- [5] R. Penrose, in *General Relativity, an Einstein Centenary Survey*, edited by S.W. Hawking and W. Israel (Cambridge University Press) (1979), p.581.
- [6] R.C. Tolman, Proc. Natl. Acad. Sci. U.S.A. **20**, 169 (1934).
- [7] H. Bondi, Mon. Not. R. Astron. Soc. **107**, 410 (1947).
- [8] D.M.Eardley and L.Smarr, Phys. Rev. **D19**, 2239 (1979).
- [9] D. Christodoulou, Commun. Math. Phys. **93**, 171 (1984).
- [10] R.P.C.A. Newman, Class. Quantum Grav. **3**, 527 (1986).
- [11] P.S. Joshi and I.H. Dwivedi, Phys.Rev. **D47**, 5357 (1993).
- [12] S.L.Shapiro and S.A.Teukolsky, Phys. Rev. Lett. **66**, 994 (1991); Phys. Rev. **D45** 2006 (1992).
- [13] A. Ori and T. Piran, Phys. Rev. **D42**, 1068, (1990).
- [14] P.S.Joshi and I.H.Dwivedi, Commun. Math. Phys. **146**, 333 (1992).
- [15] I.H. Dwivedi and P.S. Joshi, Class. Quantum Grav. **6**, 1599 (1989); **8**, 1339 (1991).
- [16] I.H. Dwivedi and P.S. Joshi, Commun. Math. Phys. **166**, 117 (1994).
- [17] P.S. Joshi and A. Krolack, Class. Quantum Grav. **13**, 3069 (1996).
- [18] U.H. Gerlach and U.K. Sengupta, Phys. Rev. **D19**, 2268 (1979).
- [19] D.S. Goldwirth and T. Piran, Phys. Rev. **D36**, 3575 (1987).
- [20] B. Waugh and K. Lake, Phys. Rev. **D40**, 2137 (1989).
- [21] C.W.Misner, K.S.Thorne, and J.A.Wheeler, *Gravitation* (Freeman, San Francisco, 1973).
- [22] C.W. Misner and D.H. Sharp, Phys. Rev. **136**, B571 (1964).
- [23] T.P. Singh and P.S. Joshi, Class. Quantum Grav. **13**, 559 (1996).
- [24] S. Jhingan, P.S. Joshi, and T.P. Singh, Class. Quantum Grav. **13**, 3057 (1996).
- [25] T. Regge and J.A. Wheeler, Phys. Rev. **108**, 1063 (1957).
- [26] E. Seidel and T. Moore, Phys. Rev. **D35**, 2287 (1987); E. Seidel, E.S. Myra and T. Moore, *ibid.* **38**, 2349 (1988).
- [27] J.M. Bardeen and T. Piran, Phys. Rep. **96**, 205 (1983).

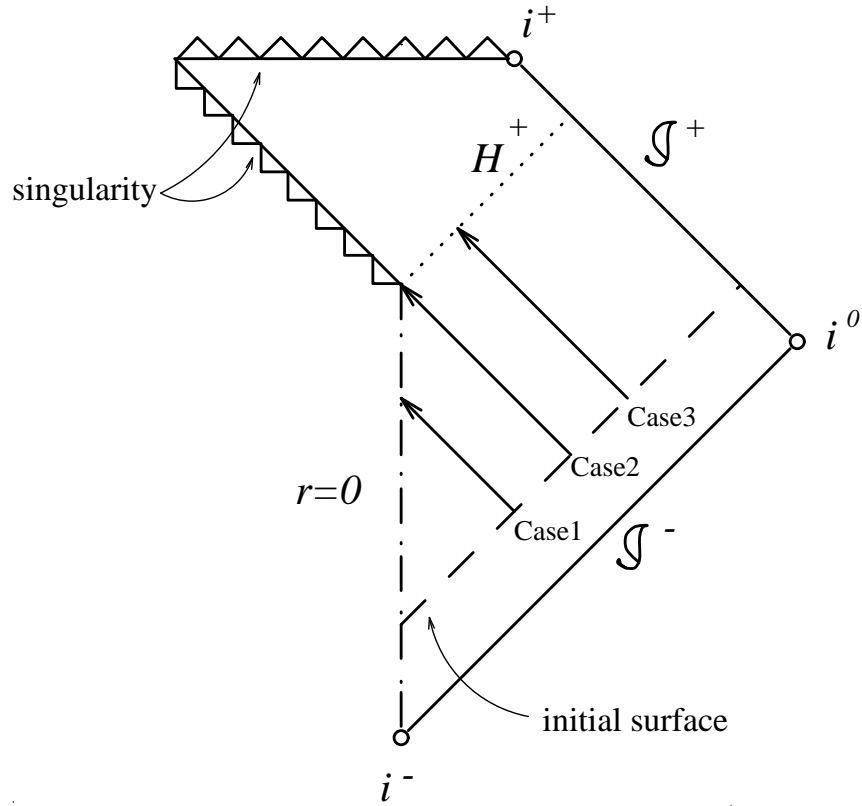


FIG. 1. Conformal diagram of the LTB space-time with a globally naked singularity. i^+ (i^-) denotes future (past) timelike infinity respectively, while i^0 denotes spacelike infinity. \mathcal{I}^+ (\mathcal{I}^-) denotes future (past) null infinity respectively. The dotted line H^+ indicates a future Cauchy horizon associated with the central naked singularity. The broken line is a null hypersurface on which we put initial wave packets. The initial positions of the wave packets are classified into Cases 1-3. For the locally naked singularity case, the Cases 1-3 are defined in the same manner as the globally naked case.

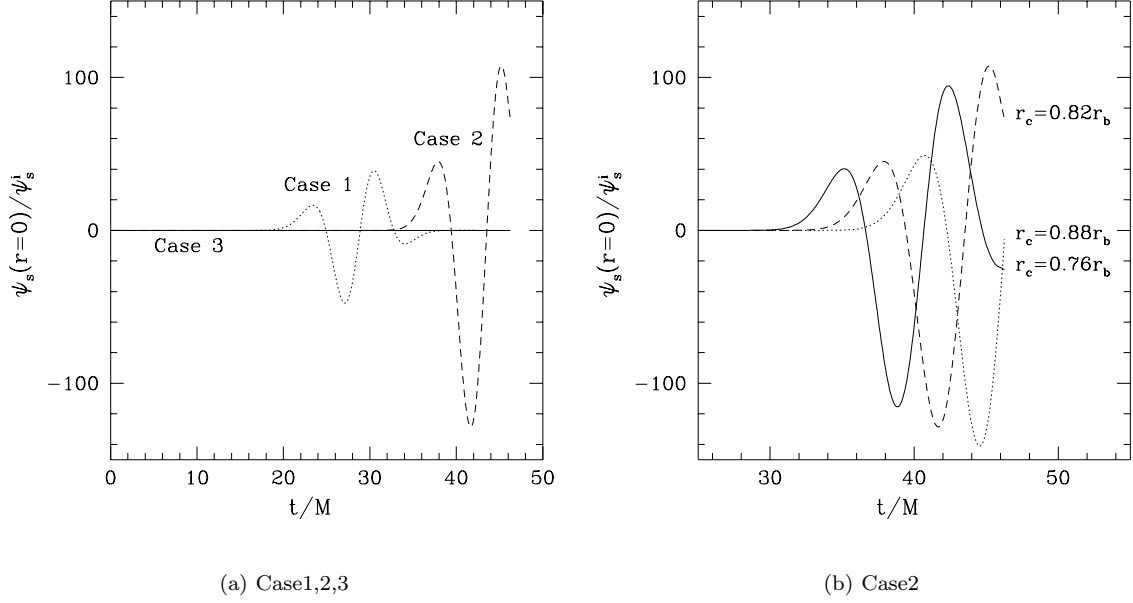


FIG. 2. Plots of the gauge-invariant variable, ψ_s , at the center, $r = 0$, with an initial width $\sigma = 0.05r_b$ for the Cases 1-3 for globally naked cases. In (a), the dotted line denotes Case 1 ($r'_c = 0.5r_b$), the broken line shows Case 2 ($r'_c = 0.82r_b$), and the solid line denotes Case 3 ($r'_c = 1.2r_b$). In (b), the results of Case 2 are shown in more detail. The broken line in (b) is the same as the broken line in (a). The solid and dotted lines show the cases that the wave packets were put on the initial surface at $r'_c = 0.76r_b$ and at $r'_c = 0.88r_b$, respectively.

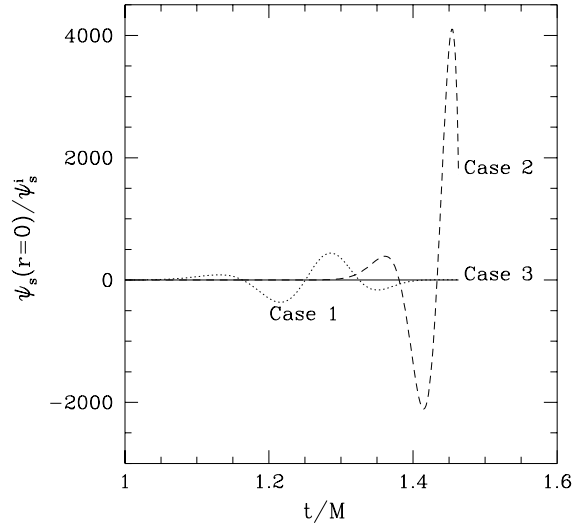


FIG. 3. Plots of the gauge-invariant variable, ψ_s , at the center, $r = 0$, with an initial width $\sigma = 0.02r_b$ for Cases 1-3 for locally naked cases. The dotted, broken, and solid lines denote Case 1 ($r'_c = 0.28r_b$), Case 2 ($r'_c = 0.38r_b$), and Case 3 ($r'_c = 0.58r_b$), respectively.

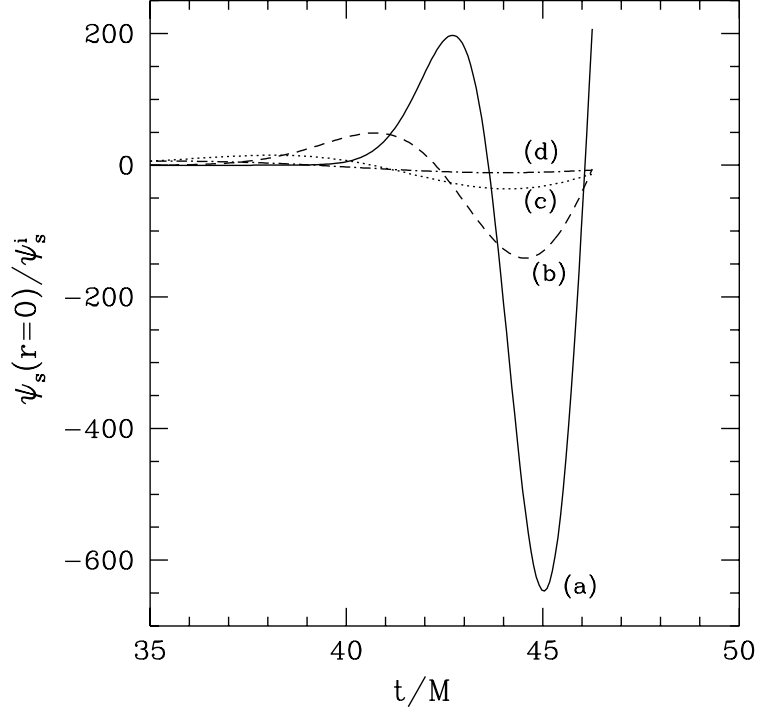


FIG. 4. Plots of the gauge-invariant variable, ψ_s , at the center, $r = 0$, in the LTB space-time for various widths of initial wave packets. The wave packets are put at $r = 0.88r_b$ on the initial null surface. The widths of initial wave packets are varied from $0.03r_b$ to $0.12r_b$. The solid line (a) corresponds to the wave form of the wave packet with the initial width $\sigma = 0.03r_b$. The broken line (b) is that of the initial width $\sigma = 0.05r_b$ while the dotted line (c) corresponds to that of the initial width $\sigma = 0.08r_b$. The broken dotted line (d) is that of the initial width $\sigma = 0.12r_b$.

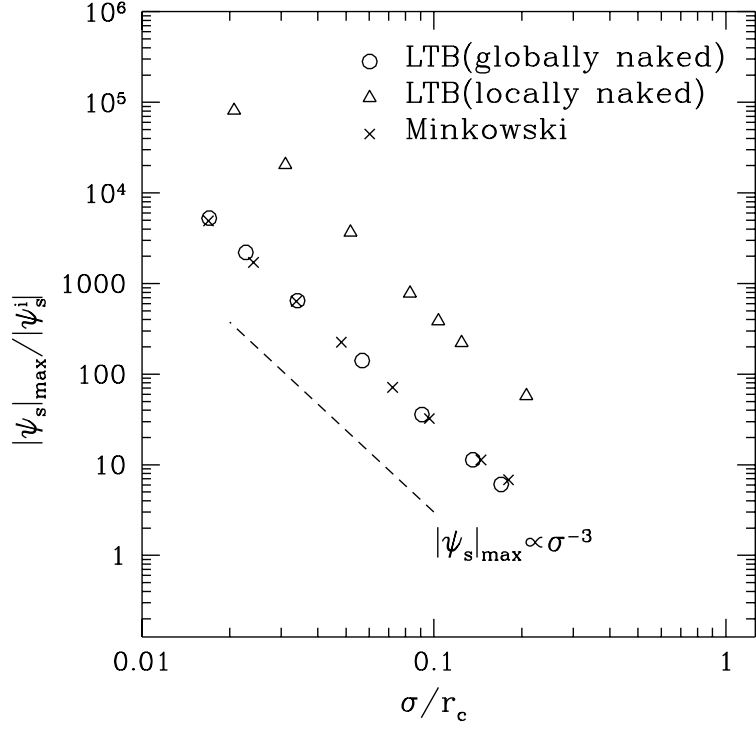
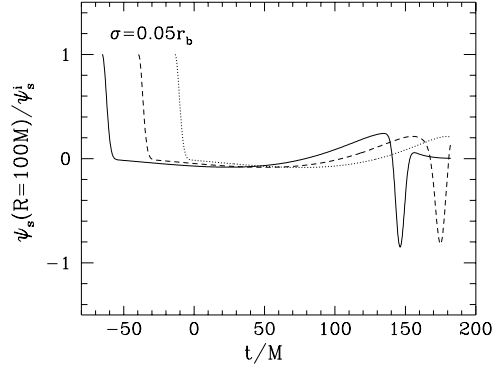
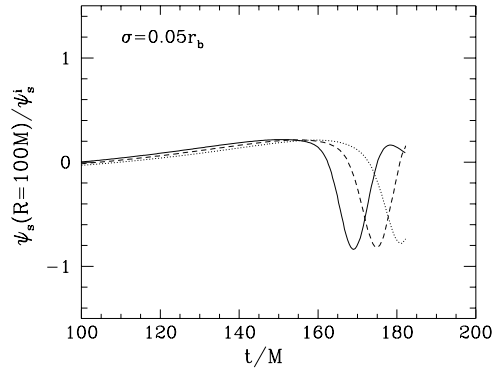


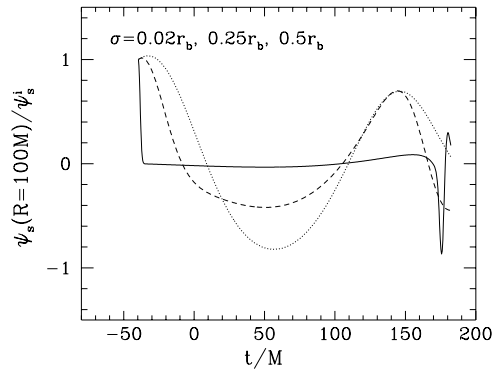
FIG. 5. The relation between the widths of initial wave packets and the maximal values of $|\psi_s|$ at the center, $r = 0$. The results for the case of the LTB space-time with globally naked singularity are marked by open circles. The results of the locally naked case are marked by the triangles. The results of the Minkowski space-time are marked by cross marks. The broken line denotes the relation, $|\psi_s|_{\max} \propto \sigma^{-3}$.



(a) Case 1,2,3

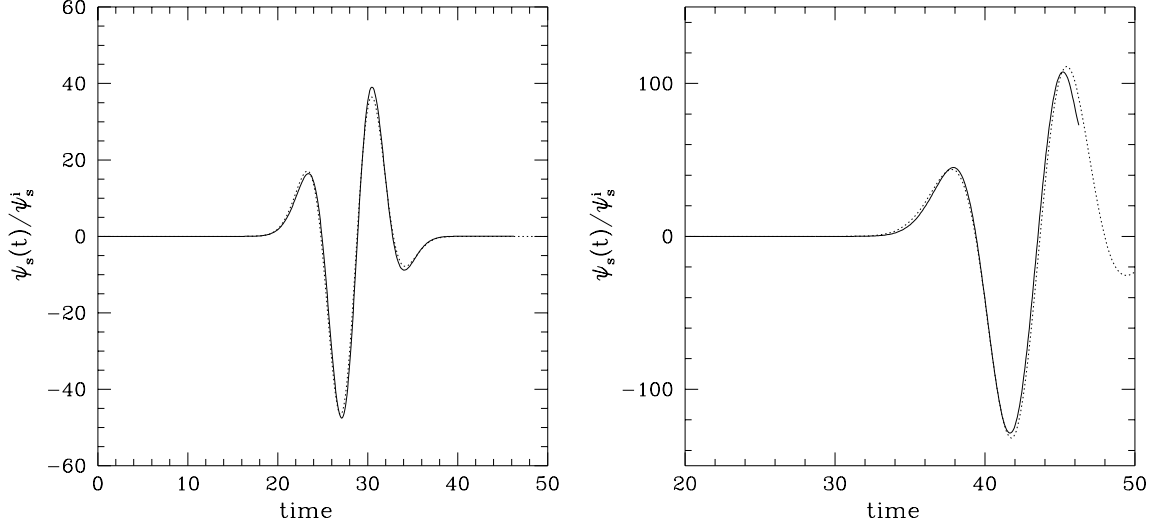


(b) Case 2



(c) $\sigma = 0.02 - 0.5r_b$ in Case2

FIG. 6. Plots of ψ_s with an initial width $\sigma = 0.05r_b$ at $R = 100M$ as a function of time, t , in the LTB space-time. In (a), the solid line shows the result for the case with an initial time when we put the wave packet on the initial surface $t_i/M = -65.310$ (Case1), the broken line is for $t_i/M = -38.529$ (Case2), the dotted line is for $t_i/M = -13.610$ (Case3). (b) depicts the details of the Case2. The solid line shows the plot of ψ_s with the initial time, $t_i/M = -34.336$, the broken line is for $t_i/M = -38.529$, the dotted line is for $t_i/M = -44.677$. We find no diverging tendency of the gauge-invariant ψ_s when it approaches the Cauchy horizon. In (c), we vary the width of the initial wave packet in Case2. The solid line is a plot of $\sigma = 0.02r_b$, the broken line is the case of the initial width $\sigma = 0.25r_b$, the dotted line is that of $\sigma = 0.5r_b$.



(a) Case 1

(b) Case 2

FIG. 7. Results of the comparison of the wave forms at the center. In (a), the solid line shows the LTB case, as a function of t/M , that is the same as the Case 1 in Fig.2(a). The dotted line shows the corresponding one of the Minkowski case, as a function of t , where $\sigma = 1.18$ and $r_c = 13.9$. In (b), the LTB case is the solid line and Case 2 in Fig.2(a). The Minkowski case is the dotted line where $\sigma = 1.25$ and $r_c = 21.4$.

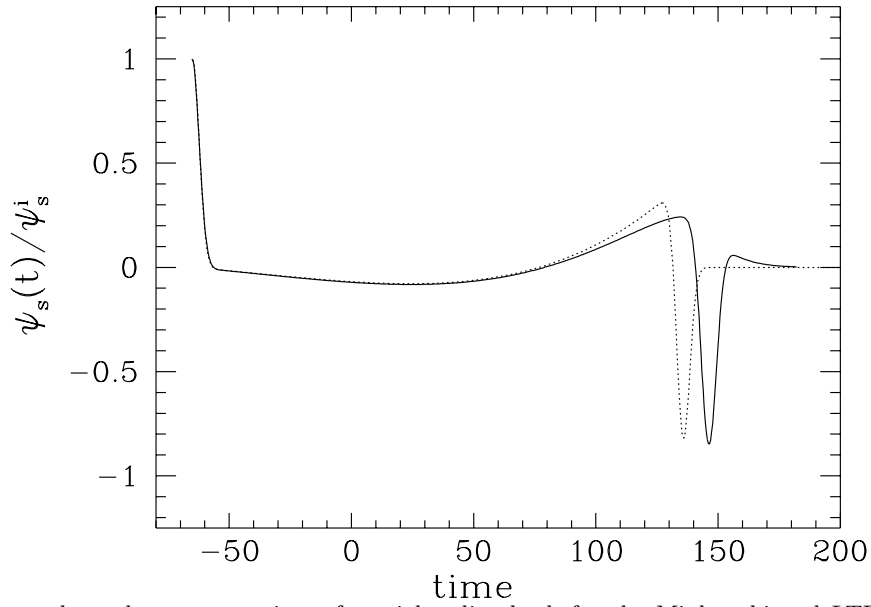


FIG. 8. Wave forms along the constant circumferential radius both for the Minkowski and LTB cases are plotted. The solid line shows the LTB case, as a function of t/M , that is identical with Case 1 in Fig.6 (a). The dotted line shows the corresponding one of the Minkowski case, as a function of t , where $\sigma = 1.33$ and $r_c = 100$.